Mycalolide B dissociates dynactin and abolishes retrograde axonal transport of dense-core vesicles

Samantha L. Cavolo[a], Chaoming Zhou[a], Stephanie A. Ketcham[b], Matthew M. Suzuki[c], Kresimir Ukalovic[c], Michael A. Silverman[c], Trina A. Schroer[b], and Edwin S. Levitan[a]
[a]Department of Pharmacology and Chemical Biology, University of Pittsburgh, Pittsburgh, PA 15261; [b]Department of Biology, Johns Hopkins University, Baltimore, MD 21218; [c]Department of Biological Sciences, Simon Fraser University, Burnaby, BC V5A 1S6, Canada

ABSTRACT **Axonal transport is critical for maintaining synaptic transmission. Of interest, anterograde and retrograde axonal transport appear to be interdependent, as perturbing one directional motor often impairs movement in the opposite direction. Here live imaging of *Drosophila* and hippocampal neuron dense-core vesicles (DCVs) containing a neuropeptide or brain-derived neurotrophic factor shows that the F-actin depolymerizing macrolide toxin mycalolide B (MB) rapidly and selectively abolishes retrograde, but not anterograde, transport in the axon and the nerve terminal. Latrunculin A does not mimic MB, demonstrating that F-actin depolymerization is not responsible for unidirectional transport inhibition. Given that dynactin initiates retrograde transport and that amino acid sequences implicated in macrolide toxin binding are found in the dynactin component actin-related protein 1, we examined dynactin integrity. Remarkably, cell extract and purified protein experiments show that MB induces disassembly of the dynactin complex. Thus imaging selective retrograde transport inhibition led to the discovery of a small-molecule dynactin disruptor. The rapid unidirectional inhibition by MB suggests that dynactin is absolutely required for retrograde DCV transport but does not directly facilitate ongoing anterograde DCV transport in the axon or nerve terminal. More generally, MB's effects bolster the conclusion that anterograde and retrograde axonal transport are not necessarily interdependent.**

Monitoring Editor
Paul Forscher
Yale University

Received: Nov 25, 2014
Revised: May 19, 2015
Accepted: May 19, 2015

INTRODUCTION

The formation and maintenance of nerve terminals depend on anterograde axonal transport from the soma. Although distinct microtubule-based motors are used for anterograde and retrograde transport, numerous studies have shown that anterograde and retrograde axonal transport exhibit interdependence. Specifically, genetic and antibody-based perturbations have shown that inhibiting kinesin, dynein, or dynactin, a large dynein accessory complex required for initiation of retrograde transport in the nerve terminal (Schroer, 2004; Lloyd *et al.*, 2012; Moughamian and Holzbaur, 2012), impedes organelle transport in both directions (Waterman-Storer *et al.*, 1997; Martin *et al.*, 1999; Deacon *et al.*, 2003; Pilling *et al.*, 2006; Haghnia *et al.*, 2007; Kwinter *et al.*, 2009; Park *et al.*, 2009). This bidirectional interdependence is not understood at the molecular level but might have great relevance to dynactin's contribution to neurological diseases (Puls *et al.*, 2003; Ström *et al.*, 2008; Farrer *et al.*, 2009).

An important organelle for synaptic function and a classic model of an anterograde cargo is the dense-core vesicle (DCV), which in neurons contains neuropeptides, secreted enzymes, and neurotrophins. Neuronal DCV function depends on its anterograde transport in axons and the nerve terminal to sites of release (e.g., synaptic boutons). However, DCVs do not move in in one direction (Wong *et al.*, 2012). Their bidirectional transport likely facilitates turnover of the presynaptic pool of DCVs and ensures uniform delivery to multiple release sites by long-distance vesicle circulation

This article was published online ahead of print in MBoC in Press (http://www.molbiolcell.org/cgi/doi/10.1091/mbc.E14-11-1564) on May 28, 2015.
The authors declare no competing financial interests.
Address correspondence to: Edwin S. Levitan (elevitan@pitt.edu).
Abbreviations used: ANF, atrial natriuretic factor; Arp1, actin-related protein 1; BDNF, brain-derived neurotrophic factor; DCV, dense-core vesicle; FRAP, fluorescence recovery after photobleaching; IP, immunoprecipitation; LatA, latrunculin A; MB, mycalolide B; SPAIM, simultaneous photobleaching and imaging.

(Wong *et al.*, 2012). Previous work implicated dynactin in bidirectional DCV transport in *Drosophila* and mammalian neurons (Kwinter *et al.*, 2009; Park *et al.*, 2009; Lloyd *et al.*, 2012; Wong *et al.*, 2012), supporting the conclusion that dynactin contributes to both directions of axonal transport to maintain nerve terminals.

However, here we report a series of experiments in mammalian hippocampal neurons and *Drosophila* sensory and motor neurons that suggests that dynactin function in axonal transport of DCVs is limited to retrograde movement. Specifically, the macrolide sponge toxin mycalolide B (MB), which depolymerizes actin filaments (F-actin; Saito *et al.*, 1994), is shown to rapidly block retrograde DCV transport in the axon and nerve terminal without affecting anterograde transport. This is not due to an effect on F-actin but instead reflects the ability of MB to dissociate the dynactin complex. Thus a novel, small-molecule dynactin inhibitor is identified to provide new evidence that anterograde and retrograde axonal transport of DCVs are not necessarily interdependent.

RESULTS

Delivery of neuropeptides to the nerve terminal is based on vesicle circulation, which includes switching from retrograde to anterograde axonal transport in the proximal axon near the soma (Wong *et al.*, 2012). To determine whether F-actin, which is abundant at the axon initial segment, is involved in this directional change, the F-actin–depolymerizing sponge macrolide toxin MB (Saito *et al.*, 1994) was applied to filleted *Drosophila* larva expressing green fluorescent protein (GFP)–tagged atrial natriuretic factor (ANF-GFP), a cargo for DCVs (Burke *et al.*, 1997; Han *et al.*, 1999; Rao *et al.*, 2001). To examine retrograde motility of DCVs, the soma and proximal axon of the lateral tracheal dendrite sensory neuron were photobleached to eliminate the signal from anterograde transport of DCVs in this region. Then retrograde transport of DCVs was monitored selectively by measuring the number of DCV puncta that appeared in the soma and proximal axon (Wong *et al.*, 2012). Remarkably, treatment with 2 μM MB for 20 min abolished this fluorescence recovery after photobleaching (FRAP; Figure 1, A and B), indicating that retrograde axonal transport of DCVs was inhibited.

To determine whether the MB effect was specific to the movement of ANF-GFP puncta in the proximal axon of *Drosophila* neurons or was due to the FRAP procedure we used, we measured transport of another DCV cargo, monomeric red fluorescent protein (mRFP)–tagged brain-derived neurotrophic factor (BDNF), in cultured rat hippocampal neuron axons with live-cell imaging (Figure 2A). Consistent with the FRAP results using ANF-GFP in *Drosophila* neurons, retrograde flux of DCVs containing BDNF-mRFP was dramatically inhibited by MB (Figure 2, A–C). However, in contrast to previous reports that anterograde and dynactin-dependent retrograde transport of axonal organelles, including DCVs, is functionally linked (Waterman-Storer *et al.*, 1997; Martin *et al.*, 1999; Pilling *et al.*, 2006; Haghnia *et al.*, 2007; Kwinter *et al.*, 2009; Park *et al.*, 2009), MB inhibition of retrograde transport occurred without inhibition of overall anterograde flux (Figure 2, B and C, and Supplemental Movie S1). Further, DCV velocity and run length were reduced only for retrograde axonal transport (Table 1). Therefore MB inhibits retrograde DCV transport while preserving anterograde transport in mammalian axons.

MB acts in vitro to depolymerize purified F-actin (Saito *et al.*, 1994). Furthermore, phalloidin labeling established that MB depolymerizes F-actin in nerve growth factor (NGF)–differentiated rat PC12 cells (Ng *et al.*, 2002a,b), which feature polarized microtubules and bidirectional DCV transport in their neurites (Lochner *et al.*, 1998; Kelley *et al.*, 2010). Therefore, to determine whether retrograde

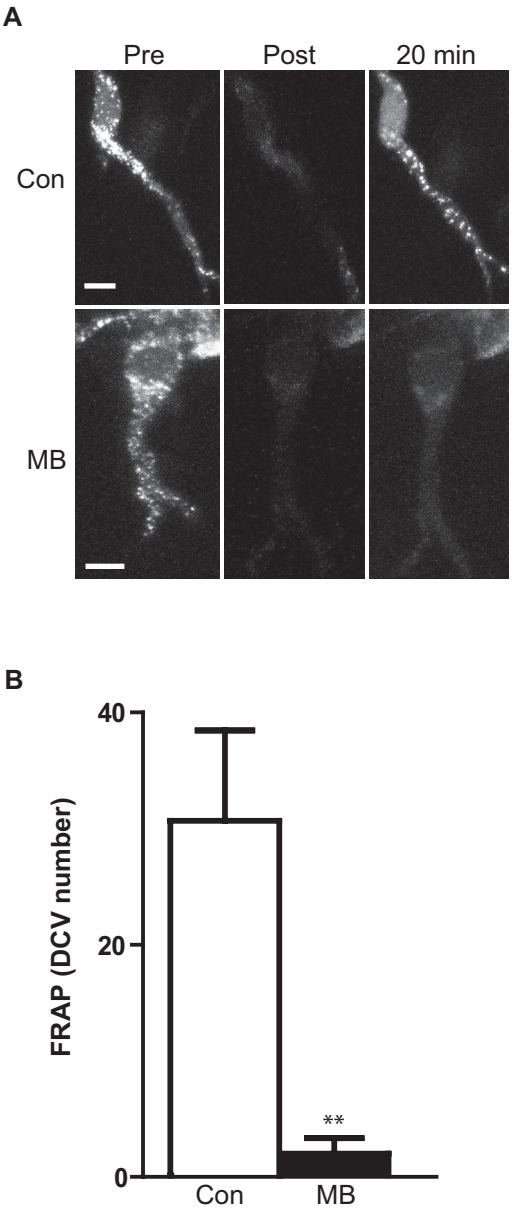

FIGURE 1: MB inhibits retrograde axonal transport of DCVs in *Drosophila*. (A) FRAP of ANF-GFP in the lateral td neuron soma and proximal axon is abolished by MB. Top, control incubation with vehicle (Con) images show FRAP in the soma and the proximal axon (the rest of the neuron is outside the field of view). Bottom, after 20 min in 2 μM MB, no FRAP is evident. Scale bar, 5 μm. (B) Quantification of FRAP by counting DCVs that entered the proximal axon and soma in 20 min after photobleaching; Con, $n = 8$; MB, $n = 6$. $^{**}p < 0.01$. Error bars represent SEM.

DCV transport inhibition by MB was due to loss of F-actin, we treated differentiated PC12 cells and hippocampal neurons with another actin poison, latrunculin A (LatA). Phalloidin labeling confirmed the loss of F-actin structures and the preservation of DCVs in both LatA-treated PC12 cells and hippocampal neurons (Figure 3, A and B). However, in contrast to the effect of MB in neurons, retrograde DCV flux in PC12 cells was not inhibited by LatA (Figure 3C). Anterograde and retrograde axonal transport of DCVs were also comparable in hippocampal neurons treated with LatA (Figure 3D and Table 1). Hence, F-actin depolymerization does not account for

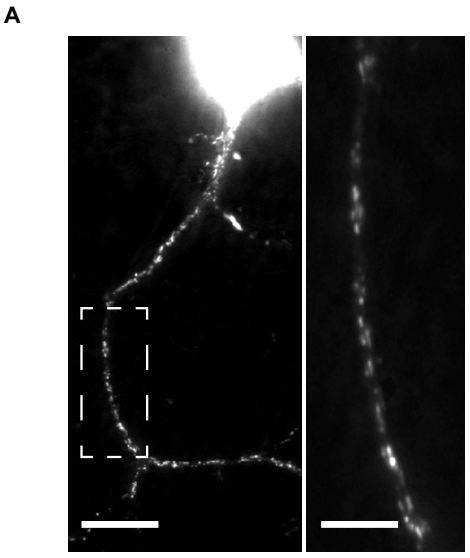

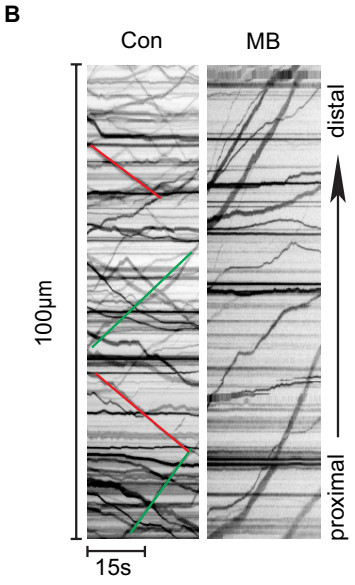

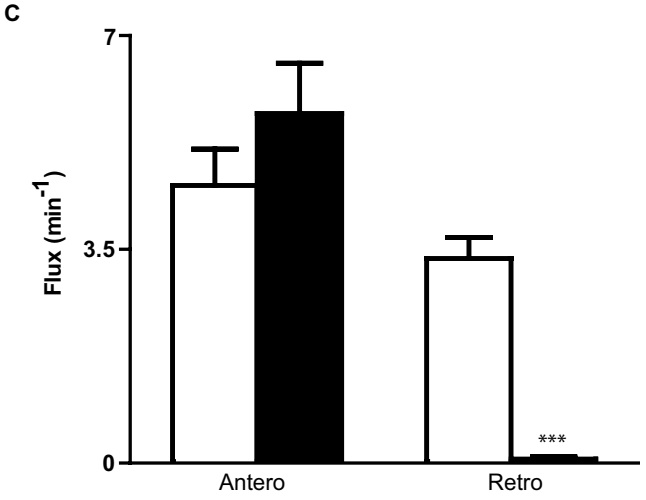

FIGURE 2: MB inhibits retrograde but not anterograde axonal transport of DCVs in cultured hippocampal neurons. (A) Left, BDNF-mRFP in hippocampal neuron soma and axon. Scale bar, 15 µm. Right, magnification of the boxed region to reveal axonal puncta. Scale bar, 2 µm. (B) Kymographs showing the MB effect on axonal transport. Green lines indicate anterograde transport, and red lines indicate retrograde transport. (C) Quantification of DCV flux in controls (Con, $n = 40$ cells) and MB ($n = 22$ cells). ***$p < 0.001$.

	Traffic values	
	Anterograde	Retrograde
Flux (min^{-1})		
Control	4.54 ± 0.58	3.35 ± 0.34
Mycalolide B	5.72 ± 0.82	0.07 ± 0.03***
Latrunculin A	4.88 ± 0.56	5.17 ± 0.62**
Velocity (µm/s)		
Control	1.37 ± 0.06	1.42 ± 0.06
Mycalolide B	1.32 ± 0.09	0.35 ± 0.13***
Latrunculin A	1.26 ± 0.03	1.36 ± 0.05
Run length (µm)		
Control	6.41 ± 0.46	5.77 ± 0.28
Mycalolide B	10.19 ± 0.88***	1.81 ± 0.81***
Latrunculin A	5.56 ± 0.34	5.74 ± 0.35

Control ($n = 40$ kymographs, 40 cells, 2414 DCVs); mycalolide B ($n = 22$ kymographs, 22 cells, 633 DCVs); latrunculin A ($n = 23$ kymographs, 23 cells, 2089 DCVs).
**$p < 0.01$, when compared with control (from each column).
***$p < 0.001$, when compared with control (from each column).

TABLE 1: DCV axonal transport parameters in hippocampal neurons.

MB's selective inhibition of retrograde DCV transport in axons and neurites, suggesting that MB might have an alternative target.

MB is chemically related to a number of F-actin–severing macrolide toxins. The amino acids that contact these toxins in rabbit skeletal muscle actin have been identified by x-ray crystallography (Klenchin *et al.*, 2003; Hirata *et al.*, 2006). Strikingly, many of these are conserved in actin-related protein 1 (Arp1), the most closely related protein to actin; for example, >80% of toxin-interacting amino acids in rabbit muscle actin are identical in rat Arp1, with the rest being conserved changes (F for Y; T for S). Arp1, which is the only actin-related protein that can form filaments, is found only as a component of dynactin, a large, multiprotein dynein accessory complex (Schroer, 2004) that facilitates efficient initiation of retrograde axonal transport of DCVs and other organelles at the distal nerve terminal ending (i.e., the most distal synaptic bouton; Lloyd et al., 2012; Moughamian and Holzbaur, 2012). Therefore we investigated whether MB affects dynactin function by measuring retrograde transport from the most distal synaptic bouton within a branch of the *Drosophila* neuromuscular junction.

Specifically, we measured the effect of MB on DCV transport in type Ib motor neuron terminals of the larval *Drosophila* neuromuscular junction. For anterograde transport, a series of distal boutons was photobleached, and FRAP was used to monitor anterograde transport into the bleached region. Specifically, flux was measured as the number of DCVs entering the photobleached region per minute. As can be seen based on the reappearance of fluorescent puncta in the photobleached region (Figure 4A) and quantification of anterograde flux (Figure 4C, black bar, Antero), MB did not affect anterograde DCV transport in the nerve terminal. To assay retrograde transport out of the most distal bouton, we used simultaneous photobleaching

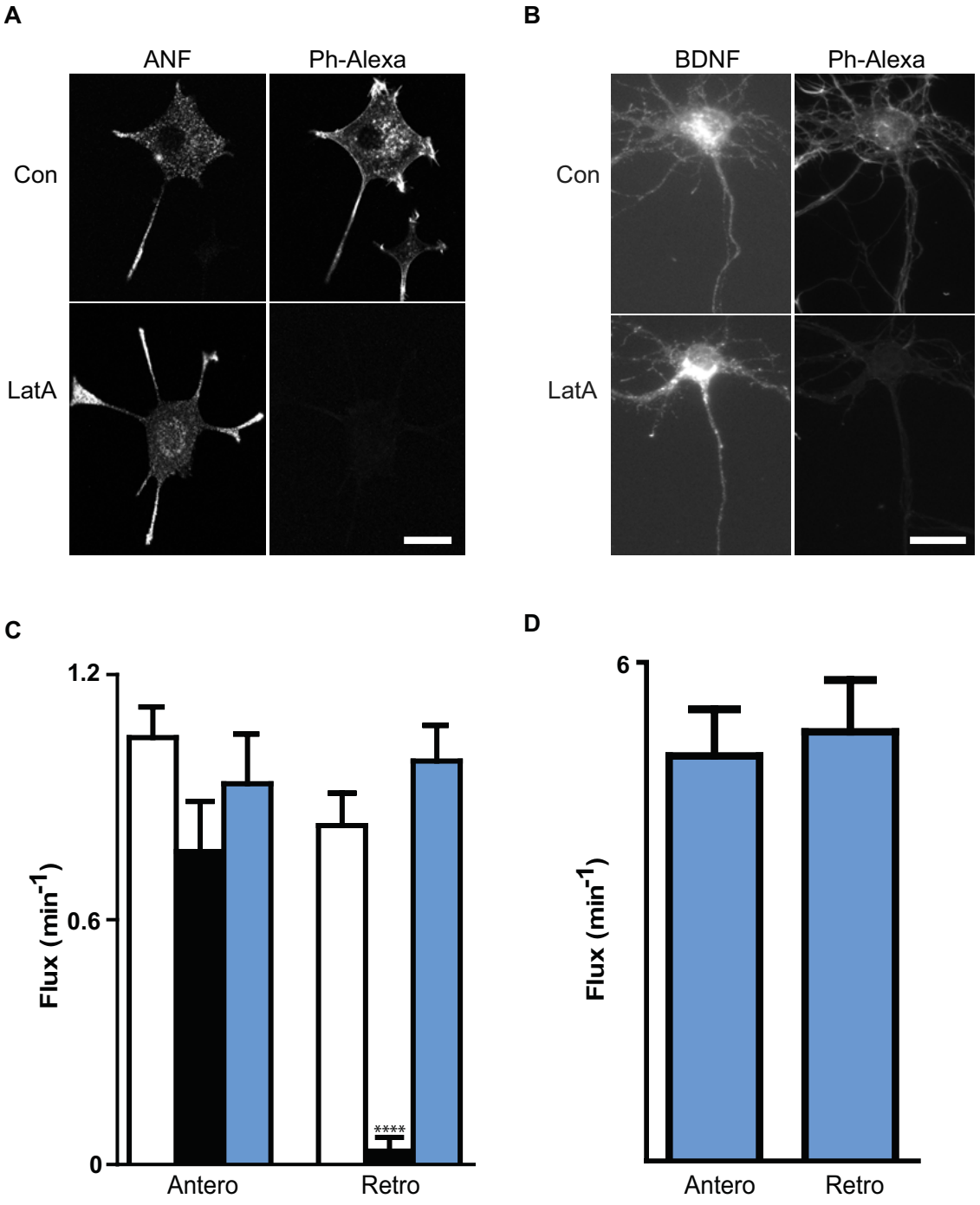

FIGURE 3: LatA does not mimic the MB effect on retrograde transport. Differentiated PC12 cells (A) and hippocampal neurons (B) expressing fluorescent protein–tagged cargoes (ANF and BDNF, respectively) were treated with vehicle (Con) or 10 µM LatA for 20 min and fixed, and then F-actin was stained with Alexa 568 (A) or 488 (B) phalloidin (Ph-Alexa). Bars, 10 µm (A), 25 µm (B). (C) Comparison of the effects of MB and LatA on anterograde and retrograde DCV flux in PC12 cell neurites. Con (open bars, $n = 13$), MB (black bars, $n = 6$), LatA (blue bars, $n = 9$). ****$p < 0.0001$. (D) Anterograde and retrograde DCV flux in LatA-treated hippocampal axons ($n = 23$). Note that retrograde flux is comparable to anterograde transport in LatA, in contrast to the dramatic decrease in retrograde transport produced by MB in hippocampal neurons (Figure 2).

and imaging (SPAIM; Wong *et al*., 2012). For these experiments, the photobleached region was restricted to a series of proximal boutons, but the most distal bouton in the terminal branch was spared. Then a photobleaching beam was positioned adjacent to the most proximal photobleached bouton to prevent FRAP by anterograde transport of DCVs to the most distal bouton (i.e., by continuous photobleaching anterogradely transported DCVs). This allowed selective measurement of retrograde DCV transport out of the most distal bouton (i.e., the flux into the photobleached region from the most distal bouton). Under control conditions, retrograde DCV transport

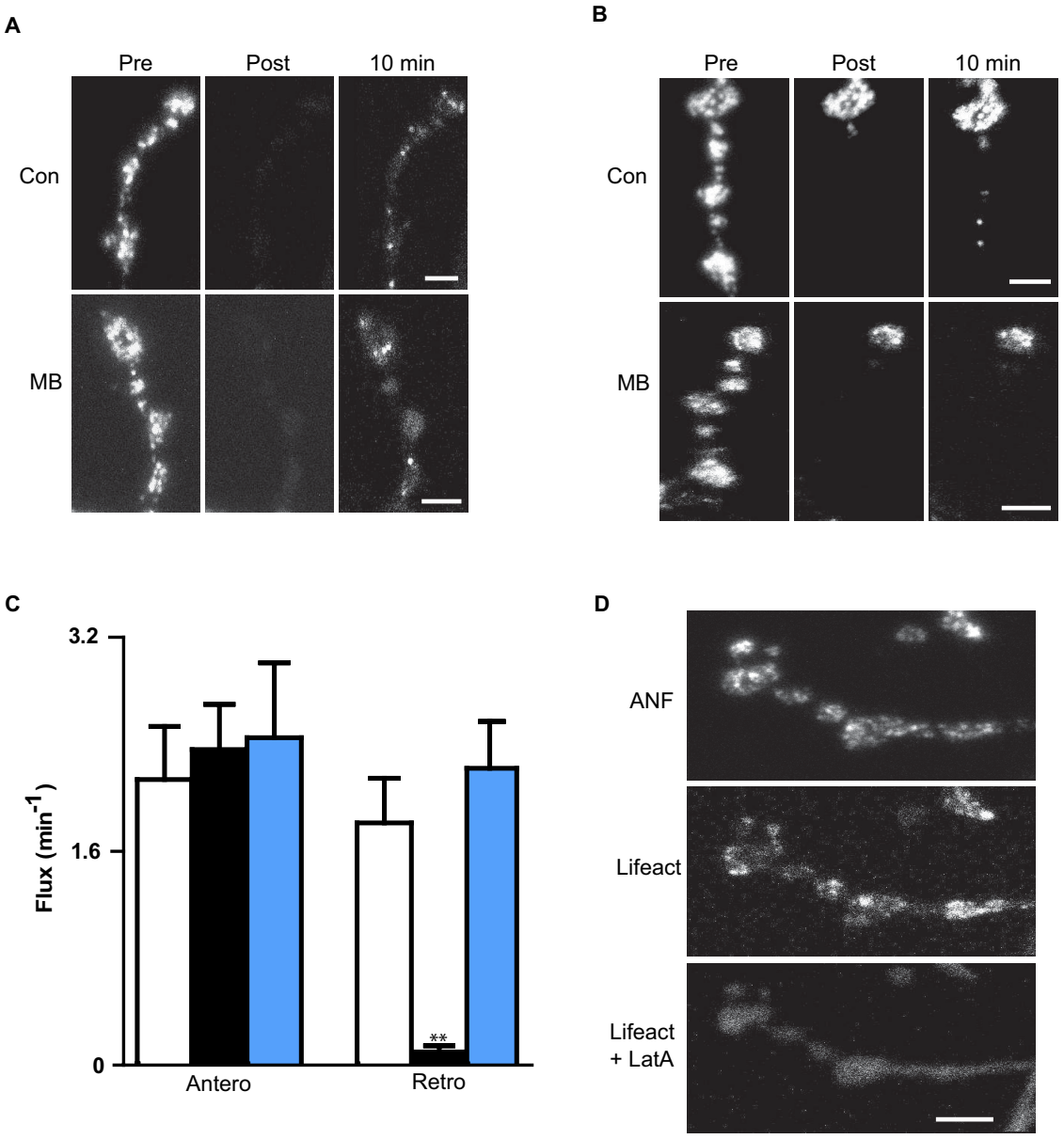

FIGURE 4: MB inhibits retrograde but not anterograde DCV transport in the nerve terminal. (A) FRAP shows that nerve terminal anterograde DCV transport is maintained in MB. ANF-GFP images from the intact neuromuscular junction are oriented with the most distal bouton at the top. Scale bar, 3 μm. (B) SPAIM shows that retrograde transport out of the most distal bouton (at top of images) is blocked by MB. Scale bar, 3 μm. (C) Quantification from time-lapse experiments of anterograde DCV flux in the terminal and retrograde DCV flux out of the most distal bouton in controls (Con, open bars, $n = 8$), MB (black bars, $n = 5$), and LatA (blue bars, $n = 4$). $^{**}p < 0.01$. (D) Lifeact-Ruby in terminal before and after treatment with LatA. Scale bar, 5 μm. ANF-GFP indicates the presence of DCVs.

out of the most distal bouton was evident (Figure 4B, top, 10 min), but after MB treatment, retrograde flux out of the most distal bouton was blocked (Figure 4, B and C). By contrast, LatA, which effectively disperses F-actin in motor neuron terminals as detected using Lifeact-Ruby (Riedl *et al.*, 2008; Hatan *et al.*, 2011; Figure 4D), affected neither retrograde DCV flux from the most distal bouton nor anterograde traffic in the terminal (Figure 4C, blue bars). To examine the reversibility of MB action, the ratio of retrograde to anterograde transport was determined immediately after MB treatment and 1 and 2 h after removal of MB from the bath. This ratio was maintained in vehicle, but MB treatment eliminated retrograde DCV transport for 2 h after its removal, showing that the MB effect is long lasting (Supplemental Figure S1). Because these results were obtained at the site where retrograde transport is initiated via dynactin (Lloyd *et al.*, 2012; Moughamian and Holzbaur, 2012), they are consistent with the hypothesis that MB inhibits dynactin activity.

Because MB depolymerizes F-actin, we hypothesized that it might also depolymerize the Arp1 filament to inhibit dynactin. Therefore we determined biochemically the effect of MB on the integrity of the dynactin complex, which also includes a single actin protomer, Arp11, CapZ α and β, p62, p25, p27, $p150^{Glued}$, p24, and dynamitin (DM) subunits (reviewed in Schroer, 2004). First, we treated PC12 cell extracts with MB and monitored dynactin integrity using immunoprecipitation of $p150^{Glued}$ followed by immunoblotting for

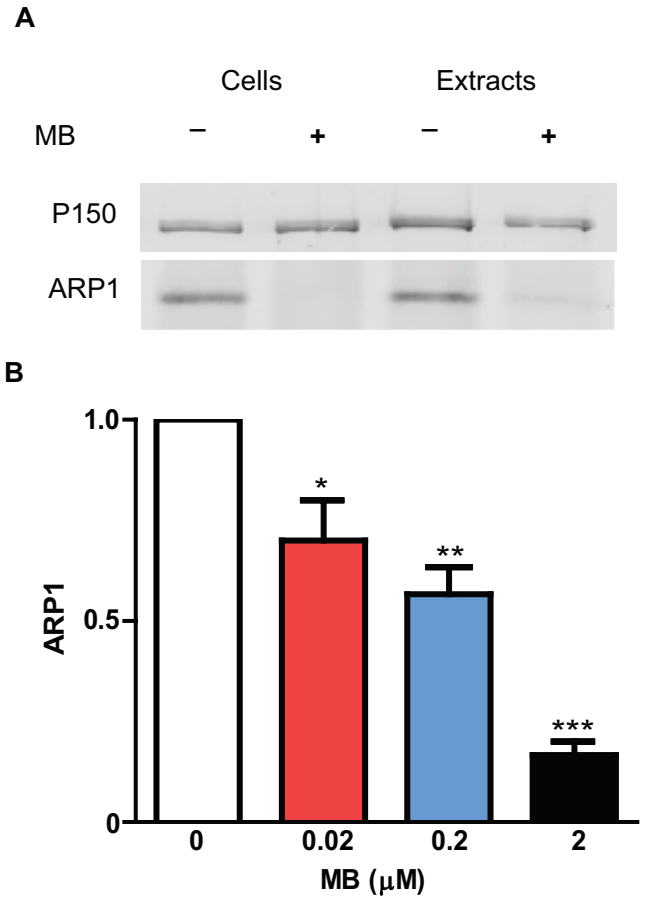

FIGURE 5: MB dissociates the dynactin complex. (A) MB blocks co-IP of Arp1 with p150^{Glued}. Vehicle or 2 μM MB was applied to PC12 cells before solubilization (Cells) or to PC12 cell extracts (Extracts). p150^{Glued} immunoprecipitates were probed for p150^{Glued} and Arp1. (B) Quantification of the concentration dependence of MB on dynactin integrity in cell extracts, assessed by co-IP with p150^{Glued}. *$p < 0.05$, **$p < 0.01$, ***$p < 0.001$.

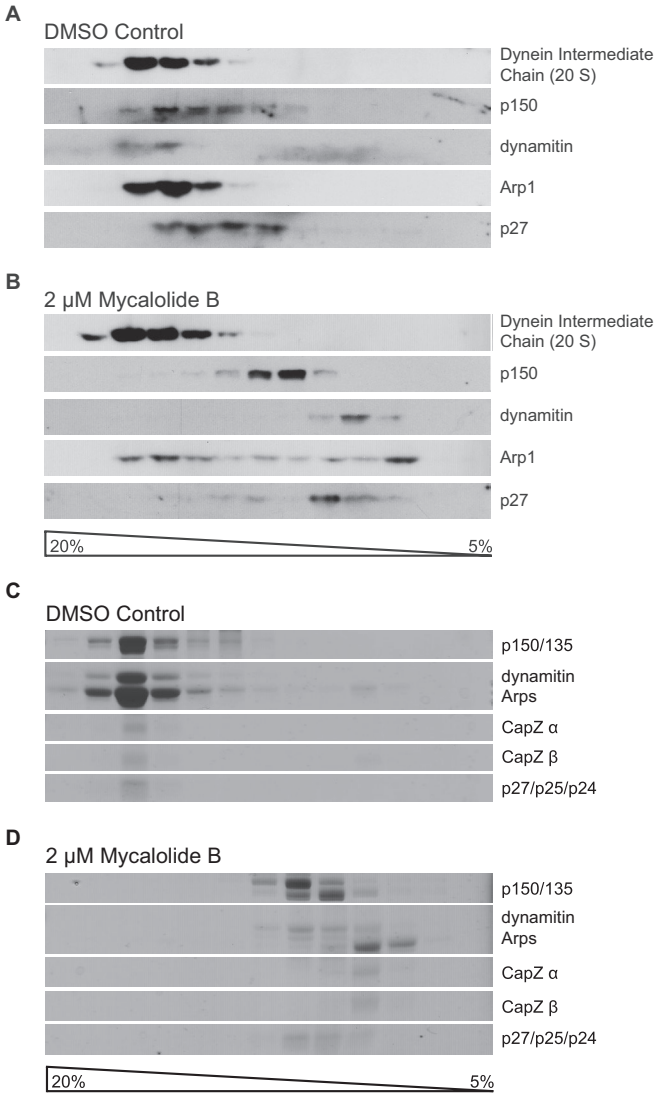

FIGURE 6: Analysis of MB on dynactin integrity by sucrose density centrifugation. (A, B) HEK293T cell lysate treated with vehicle (A) or 2 μM MB (B) was subjected to sedimentation into 5–20% sucrose gradients, and gradient fractions were analyzed by immunoblotting for dynactin subunits and the dynein IC. Densitometry indicates about half of the Arp1 in a monomer/dimer pool in the presence of MB vs. <5% in the vehicle control. (C, D) Analysis of MB on dynactin integrity in vitro. Purified bovine dynactin treated with vehicle (C) or 2 μM MB (D) was subjected to sedimentation into a 5–20% sucrose gradient, and gradient fractions were analyzed by PAGE (stained with Coomassie blue).

Arp1. Strikingly, MB profoundly diminished the amount of Arp1 co-immunoprecipitated with p150^{Glued} (Figure 5A, Extracts; $n = 5$). An effect was seen even at submicromolar concentrations (Figure 5B). MB had a similar effect when intact PC12 cells were treated with MB before washing, lysate preparation, and immunoprecipitation (Figure 5A, Cells, $n = 3$). Given that this last protocol entailed removal of MB and then dilution during generation of the cell extract and immunoprecipitation, these results suggest that the dissociation of Arp1 from p150^{Glued} induced by MB is long-lasting and possibly irreversible.

Next we used sucrose gradient sedimentation to examine the effects of MB on the stability of dynactin. To assay cellular dynactin, we treated HEK293T cell lysates with MB or vehicle (dimethyl sulfoxide [DMSO]) and fractionated using sucrose density gradient centrifugation. Dynactin subunits in the gradient fractions were then detected by immunoblotting. Dynein IC, which normally cosediments at ~20S with dynactin, was assayed as a control. In samples treated with MB, components of dynactin's shoulder–arm complex (e.g., p150^{Glued} and dynamitin) and the pointed-end complex component p27 sedimented much more slowly than in the control, indicating that they were no longer associated with each other in the dynactin complex (Figure 6, A and B). This analysis also revealed evidence of Arp1 filament disassembly by MB, as approximately half of the Arp1 sedimented very slowly (Figure 6B), suggesting dissociation of the filament to monomers or dimers. The behavior of dynein IC, by contrast, was unaffected by MB. This indicates that MB disrupts the dynactin complex while sparing the integrity of the dynein motor.

To verify that MB can act directly on dynactin, we treated purified bovine dynactin with MB before sucrose gradient sedimentation and evaluated the behavior of dynactin components in the gradient fractions via Coomassie blue staining after SDS–PAGE. This method allowed detection of additional dynactin subunits, specifically CapZ, p25, and p24 (Figure 6C). In this experiment, Arp1 sedimented in a single peak at ~6S, consistent with complete depolymerization of the filament (Figure 6D). Other components also exhibited S values consistent with dynactin disassembly (Figure 6D). We attribute the

more dramatic MB effect with purified protein than in the cell lysate to the absence of cellular actin, which would compete for MB binding. Of most importance, this analysis demonstrates that MB interacts directly with and disrupts the dynactin complex, including its Arp1 filament.

DISCUSSION

The biochemical and live-neuron imaging studies presented here lead to several new insights into dynactin and axonal transport. First, MB is a novel dynactin inhibitor that potently and directly disrupts the dynactin complex. The only other condition reported to have this effect is high concentration of the chaotropic salt potassium iodide (Eckley *et al.*, 1999). The recently published dynactin structure (Urnavicius *et al.*, 2015) provides additional insights into how MB may trigger subunit release. The predicted MB-binding site on Arp1, based on interactions of similar macrolide toxins with actin (Klenchin *et al.*, 2003; Hirata *et al.*, 2006), is immediately adjacent to the site where the dynamitin N-terminus binds Arp1. MB binding may thus dislodge dynamitin and the associated $p150^{Glued}$ and p24 components, in addition to depolymerizing the Arp1 filament itself. The identification of a rapidly acting small-molecule inhibitor will facilitate future in vitro studies of dynactin activity. MB is also potentially useful for in vivo analysis of dynactin's multiple functions (e.g., in mitosis and subcellular transport), although its effect on F-actin must of course be taken into account. Finally, MB may also be used to abolish dynactin-dependent retrograde transport to detect more easily the fate of DCVs and other organelles undergoing anterograde transport.

Second, the simplest interpretation of MB experiments is that intact dynactin is absolutely required for initiation of retrograde transport of DCVs in axons of hippocampal neurons and a *Drosophila* sensory neuron, as well as in the synaptic terminal of *Drosophila* motor neurons. This requirement (as opposed to facilitation) was not evident in living cells previously because dynactin inhibition by antibodies and genetic perturbations was incomplete. Indeed, we are not familiar with any other case in which retrograde axonal transport can be inhibited so effectively by targeting dynactin without detectable reduction of anterograde transport. The essentially complete inhibition of retrograde axonal transport of DCVs by MB suggests that no alternative mechanism exists for bypassing the requirement for dynactin in retrograde transport in the nerve terminal and axon. Even though DCVs contain bioactive peptides for release at the nerve terminal, dynactin-dependent retrograde transport is required for uniform delivery to *en passant* boutons (Wong *et al.*, 2012). Therefore our results suggest that dynactin's only contribution to the maintenance of nerve terminal anterograde cargoes (e.g., neuropeptide stores) derives from its requirement for retrograde transport.

This study also shows that anterograde DCV transport in the axon and terminal is not inhibited by dynactin complex disruption. This finding was not anticipated, because anterograde transport in intact axons and axoplasm is inhibited by genetic perturbation of dynactin and a dynactin antibody, respectively (Waterman-Storer *et al.*, 1997; Martin *et al.*, 1999; Pilling *et al.*, 2006; Haghnia *et al.*, 2007; Kwinter *et al.*, 2009; Park *et al.*, 2009). However, MB acts rapidly, which obviates the slow, indirect effects that can occur in genetic experiments, and without introducing the steric hindrance of antibody binding. A more subtle effect of dynactin on anterograde transport is suggested by the finding that MB, but not LatA, increased anterograde run length (Table 1). This further demonstrates the effectiveness of MB and suggests that dynactin has an attenuating effect on anterograde transport, which is very different from previous models. However, as no statistically significant effect was seen on anterograde flux (Table 1), the physiological importance of this observation is unclear, especially when compared with the accompanying dramatic inhibition of retrograde transport. Overall MB experiments suggest that dynactin's function in axonal transport of DCVs should be redefined from bidirectional facilitator to being strictly required for retrograde transport without a direct requirement in anterograde transport.

The independent nature of anterograde and retrograde axonal transport revealed by MB treatment is reminiscent of what is seen when the dynein regulators Nudel and LIS1 are inhibited. In these cases, retrograde axonal transport of other (but not all) organelles is preferentially inhibited (Zhang *et al.*, 2009; Yi *et al.*, 2011). Therefore there are now multiple examples in which perturbation of dynein accessory components (dynactin, LIS1, or Nudel) does not also block plus end–directed axonal transport. Our work is unique in that MB is the first rapidly acting small-molecule inhibitor of retrograde transport to yield clear evidence that retrograde and anterograde transport in the axon and nerve terminal are not mechanistically linked.

MATERIALS AND METHODS

Experimental preparations for imaging

Rat hippocampal neuronal cell culture, transfections, imaging, and image analysis were performed as described previously, with flux being derived from kymographs and normalized for length of axonal region of interest (Kwinter *et al.*, 2009). The astrocyte feeder layer for the neuronal coculture was generated using neural progenitor cells as described previously (Miranda *et al.*, 2012).

Drosophila lateral tracheal dendrite neurons (Bodmer and Jan, 1987) and muscle 6/7 type Ib motor neuron boutons were studied in UAS-ANF-GFP;386Y-GAL4 wandering third-instar larvae. To image actin with Lifeact (Riedl *et al.*, 2008), females were crossed with male UAS-Lifeact-Ruby flies (Hatan *et al.*, 2011). UAS-ANF-GFP (originally called UAS-preproANF-EMD) (Rao *et al.*, 2001) and UAS-Lifeact-Ruby are available from the Bloomington *Drosophila* Stock Center (Bloomington, IN; stocks 7001 and 35544). Imaging, FRAP, and SPAIM were performed as described previously (Levitan *et al.*, 2007; Wong *et al.*, 2012) in Ca^{2+}-free HL3 solution (in mM: 70 NaCl, 5 KCl, 0.5 Na_3–ethylene glycol tetraacetic acid [EGTA], 20 $MgCl_2$, 10 $NaHCO_3$, 5 trehalose, 115 sucrose, and 5 4-(2-hydroxyethyl)-1-piperazineethanesulfonic acid [HEPES], pH 7.2). Flux was quantified as the number of DCV puncta entering a photobleached region per minute.

PC12 Cells grown in 10% fetal bovine serum in DMEM were transfected with ANF-GFP (emerald variant; Han *et al.*, 1999) with transfectin. For DCV dynamics, cells were differentiated for 3 d with 100 µg/ml NGF before imaging at room temperature in normal saline containing (in mM) 140 NaCl, 5.4 KCl, 0.8 $MgCl_2$, 2 $CaCl_2$, 10 glucose, and 10 HEPES, pH 7.4.

Chemicals

Alexa Fluor–phalloidin (568 for PC12 and 488 for hippocampal neurons; Invitrogen, Carlsbad, CA) was used as directed by the manufacturer. DMSO 0.1% was used as the vehicle. We applied 2 µM mycalolide B (Wako, Richmond, VA) or 10 µM latrunculin A (Sigma-Aldrich, St. Louis, MO) for 20 min at room temperature for *Drosophila* and at 37°C for hippocampal neurons.

Immunoprecipitation

PC12 cells were grown for 2 d with 10% fetal bovine serum in DMEM before treatment with MB or vehicle. For treatment of intact cells, the medium was removed, cells were washed with normal saline, and MB or DMSO was added in normal saline for 20 min at room

temperature. In all immunoprecipitation (IP) experiments, cells were solubilized in 100 mM HEPES, pH 7.4, 1 mM EGTA, 2 mM $MgCl_2$, 25 mM NaCl, 0.5 mM dithiothreitol, 1% Triton X-100, 1 mM fresh phenylmethylsulfonyl fluoride (PMSF), and cOmplete Mini EDTA protease inhibitor cocktail (Roche, Indianapolis, IN). Cells were then gently scraped off from the dish on ice, debris was pelleted by centrifugation at 10,000 × *g* at 4°C for 15 min, and the supernatant was then used for IP. For extract treatments, supernatants were warmed to room temperature before adding MB or DMSO for 20 min. For immunoblot analysis, protein concentrations were measured by a bicinchoninic acid protein assay kit (Thermo Scientific, Waltham, MA) with bovine serum albumin (BSA) as a standard. Samples containing equivalents amount of protein (250–350 µg) were precleared with 30 µl of protein A/G plus agarose (Calbiochem, San Diego, CA) and then immunoprecipitated with 5 µl (250 µg/ml) of purified mouse anti-$p150^{Glued}$ antibody (BD Bioscience, San Jose, CA) overnight at 4°C. Antibody–protein complexes were precipitated with 65 µl of protein A/G plus-agarose for 3 h at 4 C. Cold 1× phosphate-buffered saline (PBS) was used to wash agarose beads five times. Protein was then eluted with 50 µl of 2× reducing electrophoresis sample buffer and used for gel electrophoresis after denaturation at 95°C for 5 min. Gels were transferred onto a Trans-Blot Transfer Medium Pure Nitrocellulose Membrane (0.2 µm; Bio-Rad, Hercules, CA), followed by electrophoresis. After blocking with 1% (wt/vol) BSA in PBST (0.1% Tween 20 in PBS) for 1 h at room temperature, the membrane was incubated 1 h at room temperature with 1 µg of anti-rabbit polyclonal against α-centractin (Arp1) antibody and 10 µl of mouse anti-$p150^{Glued}$ (250 µg/ml). Membranes were washed four times for 5 min with PBST and then incubated for 1 h at room temperature with IRDye 800CW Gt anti-rabbit immunoglobulin G (IgG; H + L) antibody and IRDye 680LT anti-mouse IgG (H + L) antibody (1:15,000; Li-COR Bioscience, Lincoln, NE). Infrared fluorescence was detected with the Odyssey Imaging System.

Sucrose density centrifugation

We incubated 50 µg of purified bovine dynactin (Bingham *et al.*, 1998) or 250–500 µg of a HEK293T cell detergent lysate (20 mM Tris, pH 7.4, 150 mM NaCl, 0.1% Triton X-100, 1 mM EGTA, 2 mM β-ME, with protease inhibitors) for 30 min at room temperature with either vehicle (DMSO, 2% of final volume) or 2 µM MB (in DMSO) in a final volume of 300–500 µl in 35 mM Tris-Cl, 5 mM $MgSO_4$, pH 7.2 (TM buffer). The samples were then layered onto 11.8 ml of 5–20% sucrose (wt/vol) gradients in TM buffer and centrifuged for 17.5 h at 34,000 rpm in an SW41 rotor. Twelve 1-ml fractions were collected from each gradient. For the purified dynactin samples, 100 µl of each fraction was subjected to trichloroacetic acid (TCA) precipitation and run on a 12.5% SDS polyacrylamide gel. For the HEK293T lysate samples, the entirety of each fraction was subjected to TCA precipitation and then run on a 12.5% SDS polyacrylamide gel and transferred to PVDF membrane for immunoblotting. The following antibodies were used to detect dynactin subunits: mouse monoclonal antibodies 150B and 45A (Quintyne *et al.*, 1999; Schafer *et al.*, 1994), mouse anti-dynamitin (BD Biosciences), and rabbit anti-DCTN6 (to p27; Proteintech Group, Chicago, IL). The mouse monoclonal antibody 74.1 (EMD Millipore, Billerica, MA) was used to detect dynein IC as a sedimentation standard and internal control.

Statistics

Error bars represent SEM. Statistical comparison for two experimental groups was based on Student's *t* test. One-way analysis of variance with Dunnett's post test was used for comparison to control for more than two experimental groups.

ACKNOWLEDGMENTS

This research was supported by National Institutes of Health Grant R01 NS32385 (to E.S.L.), the Natural Sciences and Engineering Research Council of Canada 327100-2011 (to M.A.S.), and National Institutes of Health Grant R01 GM44589 (to T.A.S.).

REFERENCES

Bingham JB, King SJ, Schroer TA (1998). Purification of dynein and dynactin from brain tissue. Methods Enzymol 298, 171–184.

Bodmer R, Jan YN (1987). Morphological differentiation of the embryonic peripheral neurons in Drosophila. Roux's Arch Dev Biol 196, 69–77.

Burke NV, Han W, Li D, Takimoto K, Watkins SC, Levitan ES (1997). Neuronal peptide release is limited by secretory granule mobility. Neuron 19, 1095–1102.

Deacon SW, Serpinskaya AS, Vaughan PS, Lopez Fanarraga M, Vernos I, Vaughan KT, Gelfand VI (2003). Dynactin is required for bidirectional organelle transport. J Cell Biol 160, 297–301.

Eckley DM, Gill SR, Melkonian KA, Bingham JB, Goodson HV, Heuser JE, Schroer TA (1999). Analysis of dynactin subcomplexes reveals a novel actin-related protein associated with the arp1 minifilament pointed end. J Cell Biol 147, 307–320.

Farrer MJ, Hulihan MM, Kachergus JM, Dächsel JC, Stoessl AJ, Grantier LL, Calne S, Calne DB, Lechevalier B, Chapon F, *et al.* (2009). DCTN1 mutations in Perry syndrome. Nat Genet 41, 163–165.

Haghnia M, Cavalli V, Shah SB, Schimmelpfeng K, Brusch R, Yang G, Herrera C, Pilling A, Goldstein LS (2007). Dynactin is required for coordinated bidirectional motility, but not for dynein membrane attachment. Mol Biol Cell 18, 2081–2089.

Han W, Ng YK, Axelrod D, Levitan ES (1999). Neuropeptide release by efficient recruitment of diffusing cytoplasmic secretory vesicles. Proc Natl Acad Sci USA 96, 14577–14582.

Hatan M, Shinder V, Israeli D, Schnorrer F, Volk T (2011). The Drosophila blood brain barrier is maintained by GPCR-dependent dynamic actin structures. J Cell Biol 192, 307–319.

Hirata K, Muraoka S, Suenaga K, Kuroda T, Kato K, Tanaka H, Yamamoto M, Takata M, Yamada K, Kigoshi H (2006). Structure basis for antitumor effect of aplyronine A. J Mol Biol 356, 945–954.

Kelly TA, Katagiri Y, Vartanian KB, Kumar P, Chen II, Rosoff WJ, Urbach JS, Geller HM (2010). Localized alteration of microtubule polymerization in response to guidance cues. J Neurosci Res 88, 3024–3033.

Klenchin VA, Allingham JS, King R, Tanaka J, Marriott G, Rayment I (2003). Trisoxazole macrolide toxins mimic the binding of actin-capping proteins to actin. Nat Struct Biol 12, 1058–1063.

Kwinter DM, Lo K, Mafi P, Silverman MA (2009). Dynactin regulates bidirectional transport of dense-core vesicles in the axon and dendrites of cultured hippocampal neurons. Neuroscience 162, 1001–1010.

Levitan ES, Lanni F, Shakiryanova D (2007). In vivo imaging of vesicle motion and release at the Drosophila neuromuscular junction. Nat Protoc 2, 1117–1125.

Lloyd TE, Machamer J, O'Hara K, Kim JH, Collins SE, Wong MY, Sahin B, Imlach W, Yang Y, Levitan ES, *et al.* (2012). The p150(Glued) CAP-Gly domain regulates initiation of retrograde transport at synaptic termini. Neuron 74, 344–360.

Lochner JE, Kingma M, Kuhn S, Meliza CD, Cutler B, Scalettar BA (1998). Real-time imaging of the axonal transport of granules containing a tissue plasminogen activator/green fluorescent protein hybrid. Mol Biol Cell 9, 2463–2476.

Martin M, Iyadurai SJ, Gassman A, Gindhart JG Jr, Hays TS, Saxton WM (1999). Cytoplasmic dynein, the dynactin complex, and kinesin are interdependent and essential for fast axonal transport. Mol Biol Cell 10, 3717–3728.

Miranda CJ, Braun L, Jiang Y, Hester ME, Zhang L, Riolo M, Wang H, Rao M, Altura RA, Kaspar BK (2012). Aging brain microenvironment decreases hippocampal neurogenesis through Wnt-mediated survivin signaling. Aging Cell 11, 542–552.

Moughamian AJ, Holzbaur EL (2012). Dynactin is required for transport initiation from the distal axon. Neuron 74, 331–343.

Ng YK, Lu X, Levitan ES (2002a). Physical mobilization of secretory vesicles facilitates neuropeptide release by nerve growth factor-differentiated PC12 cells. J Physiol 542, 395–402.

Ng YK, Lu X, Watkins SC, Ellis-Davies GC, Levitan ES (2002b). Nerve growth factor-induced differentiation changes the cellular organization

of regulated peptide release by PC12 cells. J Neurosci 22, 3890–3897.
Park JJ, Koshimizu H, Loh YP (2009). Biogenesis and transport of secretory granules to release site in neuroendocrine cells. J Mol Neurosci 37, 151–159.
Pilling AD, Horiuchi D, Lively CM, Saxton WM (2006). Kinesin-1 and dynein are the primary motors for fast transport of mitochondria in Drosophila motor axons. Mol Biol Cell 17, 2057–2068.
Puls I, Jonnakuty C, LaMonte BH, Holzbaur EL, Tokito M, Mann E, Floeter MK, Bidus K, Drayna D, Oh SJ, *et al.* (2003). Mutant dynactin in motor neuron disease. Nat Genet 33, 455–456.
Quintyne NJ, Gill SR, Eckley DM, Crego CL, Compton DA, Schroer TA (1999). Dynactin is required for microtubule anchoring at centrosomes. J Cell Biol 147, 321–334.
Rao S, Lang C, Levitan ES, Deitcher DL (2001). Visualization of neuropeptide expression, transport, and exocytosis in Drosophila melanogaster. J Neurobiol 49, 159–172.
Riedl J, Crevenna AH, Kessenbrock K, Yu JH, Neukirchen D, Bista M, Bradke F, Jenne D, Holak TA, Werb Z, *et al.* (2008). Lifeact: a versatile marker to visualize F-actin. Nat Methods 5, 605–607.
Saito S, Watabe S, Ozaki H, Fusetani N, Karaki H (1994). Mycalolide B, a novel actin depolymerizing agent. J Biol Chem 269, 29710–29714.
Schafer DA, Gill SR, Cooper JA, Heuser JE, Schroer TA (1994). Ultrastructural analysis of the dynactin complex: an actin-related protein is a component of a filament that resembles F-actin. J Cell Biol 126, 403–412.
Schroer TA (2004). Dynactin. Annu Rev Cell Dev Biol 20, 759–779.
Ström AL, Shi P, Zhang F, Gal J, Kilty R, Hayward LJ, Zhu H (2008). Interaction of amyotrophic lateral sclerosis (ALS)-related mutant copper-zinc superoxide dismutase with the dynein-dynactin complex contributes to inclusion formation. J Biol Chem 283, 22795–22805.
Urnavicius L, Zhang K, Diamant AG, Motz C, Schlager MA, Yu M, Patel NA, Robinson CV, Carter AP (2015). The structure of the dynactin complex and its interaction with dynein. Science 347, 1441–1446.
Waterman-Storer CM, Karki SB, Kuznetsov SA, Tabb JS, Weiss DG, Langford GM, Holzbaur EL (1997). The interaction between cytoplasmic dynein and dynactin is required for fast axonal transport. Proc Natl Acad Sci USA 94, 12180–12185.
Wong MY, Zhou C, Shakiryanova D, Lloyd TE, Deitcher DL, Levitan ES (2012). Neuropeptide delivery to synapses by long-range vesicle circulation and sporadic capture. Cell 148, 1029–1038.
Yi JY, Ori-McKenney KM, McKenney RJ, Vershinin M, Gross SP, Vallee RB (2011). High-resolution imaging reveals indirect coordination of opposite motors and a role for LIS1 in high-load axonal transport. J Cell Biol 195, 193–201.
Zhang Q, Wang F, Cao J, Shen Y, Huang Q, Bao L, Zhu X (2009). Nudel promotes axonal lysosome clearance and endo-lysosome formation via dynein-mediated transport. Traffic 10, 1337–1349.